

See discussions, stats, and author profiles for this publication at: <https://www.researchgate.net/publication/268926250>

# Controlling the Catalytic Efficiency on the Surface of Hollow Gold Nanoparticles by Introducing an Inner Thin Layer of Platinum or Palladium

ARTICLE in JOURNAL OF PHYSICAL CHEMISTRY LETTERS · NOVEMBER 2014

Impact Factor: 7.46 · DOI: 10.1021/jz502071v

---

CITATIONS

5

READS

100

---

## 3 AUTHORS:



Mahmoud A. Mahmoud

Georgia Institute of Technology

76 PUBLICATIONS 1,807 CITATIONS

[SEE PROFILE](#)



Batyr Garlyyev

Georgia Institute of Technology

5 PUBLICATIONS 20 CITATIONS

[SEE PROFILE](#)



Mostafa A El-Sayed

Georgia Institute of Technology

676 PUBLICATIONS 55,276 CITATIONS

[SEE PROFILE](#)

# Controlling the Catalytic Efficiency on the Surface of Hollow Gold Nanoparticles by Introducing an Inner Thin Layer of Platinum or Palladium

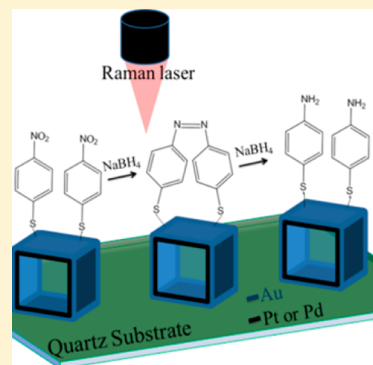
Mahmoud A. Mahmoud, Batyr Garlyyev, and Mostafa A. El-Sayed\*

Laser Dynamics Laboratory, School of Chemistry and Biochemistry, Georgia Institute of Technology, Atlanta, Georgia 30332-0400, United States

## Supporting Information

**ABSTRACT:** The efficiency of heterogeneous catalysis of electron-transfer reactions on the surface of gold nanoshells was changed by adding an inner platinum or palladium nanoshell in the double-shell nanocatalysts. The reduction of 4-nitrothiophenol (4NTP) by borohydride was studied as a model reaction. To confirm the heterogeneous catalytic mechanism, the nanocatalysts were assembled into a monolayer on the surface of a quartz substrate using the Langmuir–Blodgett technique, and the 4NTP was allowed to bind to the surface of gold through a strong thiol bond. The stages of the reduction reaction of 4NTP on the surface of gold were successfully followed by time-resolved surface-enhanced Raman spectroscopy. Palladium was found to increase the catalytic efficiency of the gold surface due to the presence of a new Fermi level of the palladium–gold alloy, while platinum decreased its catalytic efficiency due to the electron-withdrawing effect of platinum atoms, which resulted from the difference in their electrochemical reduction potentials.

**SECTION:** Surfaces, Interfaces, Porous Materials, and Catalysis



Nanoparticles are characterized by their high surface to volume ratio; this large surface area of the nanoparticles increases their efficiency when used for catalysis.<sup>1–3</sup> Introducing sharp corners and edges to the shape of the nanocatalysts further increases their catalytic efficiency.<sup>4</sup> As the activity of the nanocatalyst depends on the number of high-energy active centers,<sup>5</sup> atoms located at the sharp tips are thermodynamically and catalytically active because they are unsatisfied in valency.<sup>6</sup> Although the nanocatalysts with sharp tips present good enhancement of the catalytic efficiency, their sharp ends become rounded after the catalytic reaction, which causes a remarkable decrease in the catalytic efficiency.<sup>7</sup> The shape change of the nanocatalyst could be due to leaching or rearrangement of the atoms located on its sharp ends.<sup>7</sup>

Confinement of the reacting materials within the nanocatalysts has been found to improve their catalytic efficiency.<sup>8–15</sup> This confinement is acquired either by designing the nanocatalyst to have a cavity or by fixing the catalyst on the surface of the inside wall of an inert support of containing voids. Nanocage catalysts made of a single metal such as gold, platinum, and palladium or two metals, such as double-shell structures of gold–platinum, gold–palladium, and platinum–palladium, have presented high catalytic efficiency due to the cage effect.<sup>8–11</sup> The idea of cage catalysis was supported by comparing the catalytic efficiency of gold nanocages with that of the solid nanocatalyst of similar shape, and the gold nanocages were found to have a higher catalytic efficiency than the solid nanocatalyst.<sup>16,17</sup> The cage effect was also observed for palladium nanotubes, which showed a high catalytic efficiency

for the Suzuki reaction.<sup>12</sup> Additionally, silver oxide prepared in situ on the interior wall of gold nanocages showed high photocatalytic activity for the decomposition of an organic dye as the reactive radicals were confined inside of the gold nanocage.<sup>18</sup> High catalytic performance was also observed for hydrogen generation from formic acid on the surface of gold nanoparticles encapsulated in silica nanospheres.<sup>13</sup> The density functional theoretical calculation related the high catalytic efficiency of the hollow nanocatalysts to the electronic confinement effect.<sup>19</sup> Nanocatalysts fixed on the inner wall of porous metal–organic frameworks (MOFs) showed high catalytic activity due to the confinement of the reactant inside of the voids present in the structure of the MOFs.<sup>20</sup> Polymer nanofibers when used as a support for platinum and ruthenium nanocatalysts showed high catalytic efficiency due to the cage effect.<sup>21</sup> Nickel, cobalt, iron, and their respective oxides encapsulated inside of a SiO<sub>2</sub> nanoshell showed an exciting catalytic performance and thermal stability during the catalytic run at high temperature.<sup>14</sup> High electrocatalytic efficiency was also observed in hybrid inorganic nanostructures such as ruthenium and Cu<sub>3</sub>S due to their high surface area and exciting electronic properties.<sup>22</sup>

Due to the small size of the nanocatalysts, which in some cases approaches the size of the reacting materials, the

**Received:** September 29, 2014

**Accepted:** November 12, 2014

**Published:** November 12, 2014

mechanism of the nanocatalysis is not clearly understood. In fact, heterogeneous catalysis is suggested when the catalysis takes place on the surface of the nanocatalyst, while a homogeneous mechanism is favored when the catalysis proceeds through the formation of a complex, either on or far from the surface of the catalysts. Raman spectroscopy presents fingerprint vibrational spectra for molecules. Plasmonic nanoparticles are characterized by the presence of an electromagnetic field when they interact with light of resonant frequency; this plasmon field is able to enhance the Raman signal of molecules located in its domain, as in surface-enhanced Raman spectroscopy (SERS). SERS is a sensitive technique that is able to sense concentrations down to the zeptomolar range ( $10^{-21}$ ).<sup>23</sup> The high sensitivity of SERS has made it possible to use this technique to probe the catalytic reaction as it proceeded on the surface of the plasmonic nanocatalyst.<sup>24,25</sup>

This Letter aims to study the mechanism of the heterogeneous catalysis on the surface of gold nanoshells when present as a single nanoshell and when combined with an inner platinum or palladium nanoshell into a double-shell nanostructure. As it is not easy to differentiate between homogeneous and heterogeneous catalysis by the colloidal nanoparticles, three considerations were taken into account to ensure a heterogeneous mechanism during the design of the experiment: (1) In order to fix the nanocatalysts, they were assembled into a monolayer on the surface of a quartz substrate by the Langmuir–Blodgett (LB) technique, (2) the reduction of 4-nitrothiophenol (4NTP) by borohydride (BH) was used as a model reaction with the 4NTP bound to the surface of the nanocatalyst through a strong gold–thiol bond, and (3) the highly sensitive SERS technique was used to follow the reaction on the surface of the gold nanoparticles so the Raman signal recorded would be for the molecules bound to or near the surface of the gold, where the plasmon field is strong. This experimental design made it possible to study the mechanism of the heterogeneous catalysis on the surface of the gold nanoshells and also to study the effect of hybridizing of the electronic properties of gold, with either platinum or palladium, on the catalytic efficiency of the gold surface. Cyclic voltammetry measurements were used to confirm the kinetic results obtained from the catalysis experiments.

Gold nanocage, gold–platinum double-shell, and gold–palladium double-shell nanocatalysts were prepared from a silver nanocubes template by the galvanic replacement technique, as previously reported (for the detailed procedure, see the Supporting Information).<sup>8</sup> In order to assemble the nanocatalysts into monolayers on the surface of the quartz substrate, the prepared nanoparticles in aqueous solution were transferred to chloroform. Then, 100 mL from the nanocatalyst solution was precipitated by centrifugation at 6000 rpm for 10 min and redispersed in 2 mL of methanol. The nanoparticles in methanol were diluted with 3 mL of chloroform. The nanoparticles were then dispersed on top of the Nima 611D LB trough using a microsyringe filled with a water sublayer. The nanocatalyst monolayer was dried for 30 min before being transferred to the surface of the quartz substrate by the vertical dipping technique. Eight quartz substrates of  $1\text{ cm} \times 2.5\text{ cm}$  were coated simultaneously at a surface pressure of  $2\text{ mN/m}$ , which was measured by a D1L-75 model pressure sensor. In order to coat the surface of the nanocatalysts with 4NTP, substrates coated with nanocatalysts were immersed in a  $0.1\text{ mM}$  aqueous solution of 4NTP and left overnight. The

substrates were washed five times in deionized (DI) water by immersion and gentle shaking. The substrates were then immersed in a  $1\text{ mM}$  sodium BH solution and removed after different soaking times for Raman analysis using a Renishaw In via Raman microscope. For the cyclic voltammetry measurements, 10 mL of aqueous nanocatalyst solutions were mixed with 1 mL of an aqueous 4NTP solution and left overnight. Then, the solution was centrifuged twice at 6000 rpm for 10 min to remove excess 4NTP. The nanoparticles with 4NTP on the surface were drop-casted on a glass carbon electrode. A AgCl/Ag electrode was used as the reference electrode, and platinum was used as a counter electrode. All of the cyclic voltammetry measurements were carried out in  $0.5\text{ M H}_2\text{SO}_4$  at a scan rate of  $50\text{ mV/s}$ . A Zeiss Ultra 60 microscope was used for the scanning electron microscopy (SEM) imaging. A Tecnai F30 microscope was used for high-resolution transmission electron microscopy (HR-TEM) imaging and energy-dispersive X-ray spectroscopy (EDS) mapping.

*Characterization and Monolayer Assembly of the Hollow Nanocatalysts.* The efficiency of heterogeneous catalysts depends on the crystal structure and the surface potential energy. The reactions in this study take place on the surface of gold even in the case of AuPdNCs and AuPtNCs. It is useful to study the crystal structures of the double-shell nanocatalysts and monitor how the two metal shells are arranged. Figure 1A shows a high-resolution TEM image of part of the wall of a single AuNC. One gold shell was observed in the image. AuPdNCs, alternatively, seem to have three different layers. The outer layer is pure gold, the inner layer is pure palladium, while the middle layer is a gold–palladium alloy (see Figure 1B). Gold and palladium have a face-centered cubic (fcc) lattice; the  $d$ -spacing of the  $\{111\}$  facet of gold is  $0.23\text{ nm}$ , which is comparable with that of palladium ( $0.2\text{ nm}$ ). The comparable lattice parameters of gold and palladium make their alloying quite possible. Figure 1C shows the TEM image of the wall of AuPtNC; the gold atoms in the outer gold layer are well organized, while the interfacial layer between the platinum and gold is rough because platinum and gold do not form a homogeneous alloy. Indeed, platinum has a fcc lattice, and the  $d$ -spacing of the  $\{111\}$  facet is  $0.27\text{ nm}$ , which is much larger than that of gold, preventing the alloy formation and generating a strong lattice strain in the interfacial layer. For more careful characterization of the hollow nanocatalysts, EDS mapping was carried out for AuPdNCs (see Figure 1D). As shown from the EDS elemental mapping image, AuPdNC is composed of palladium and gold metals, where the gold appears as an outer shell with green color in the image, while the palladium inner shell that appeared with red color is located inside of the cage, and the alloy between the inner and outer shells is shown in yellow. EDS mapping images of the individual metals are shown in the center of Figure 1D.

In order to increase the accuracy of the heterogeneous catalysis experiments, the LB technique was used to assemble the nanocatalysts into a monolayer on the surface of a quartz substrate. The LB assembly keeps the nanocatalyst fixed in an organized way during the catalysis experiment. Figure 2A–C shows the SEM images of AuNC, AuPdNC, and AuPtNC monolayers assembled on the surface of quartz substrates at a surface pressure of  $2\text{ mN/m}$ . The localized surface plasmon resonance extinction spectrum of the nanocatalysts after assembling on the surface of a quartz substrate are shown in Figure S1 (Supporting Information).

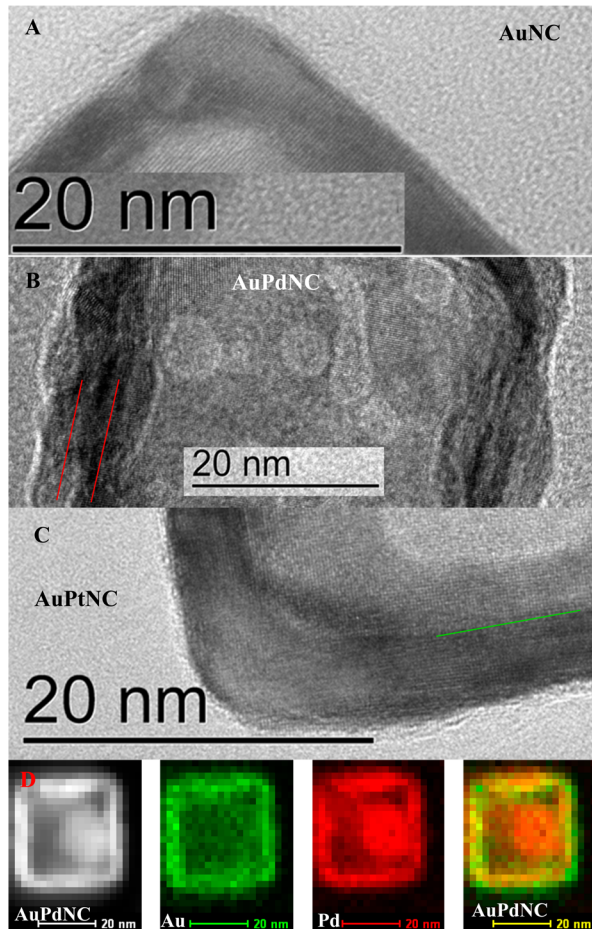


**Figure 1.** HR-TEM images of the wall of the (A) gold nanocage, (B) gold–palladium double-shell nanoparticle, and (C) gold–platinum double-shell nanoparticle. It is clear that the gold nanocage has one crystalline wall, while the gold–palladium double-shell has three different layers, two of them for pure gold and pure palladium shells and an alloy layer in between, the alloy layer located between the two red lines in the image. In the case of the gold–platinum double-shell nanoparticle, two layers are observed that are separated by the green line because platinum and gold cannot form a homogeneous alloy, while palladium and gold mix well because they have comparable crystal lattice parameters. (D) EDS elemental mapping of AuPdNC of bright color (left image); the gold atoms of green color appear as an outer shell, while palladium atoms of red color are shown as an inner shell (right image). The EDS mapping images of the individual palladium and gold before convolution are in the center.

**Spectroscopic Study of Catalytic Reactions on the Surface of Gold Nanoshells.** BH reduces 4NTP into 4-aminothiophenol (4ATP) on the surface of certain metal catalysts. On the basis of theoretical simulations, this reaction likely proceeds through the formation of an intermediate dimeric azo compound. This slightly persistent intermediate may undergo further reduction into 4ATP. The azo dimer was observed experimentally arising from a photochemical reaction rather than through a thermal mechanism.<sup>26</sup> In order to eliminate the photochemical reaction that could take place as a result of the Raman laser irradiation, 4NTP adsorbed on the surface of the nanocatalysts was exposed to the laser for different periods of time. No change was observed in the SERS spectrum of 4NTP due to the irradiation, which suggested that no photochemical reaction is possible by such low-energy excitation photons (see Figure S2, Supporting Information). In multiple-step electron-transfer

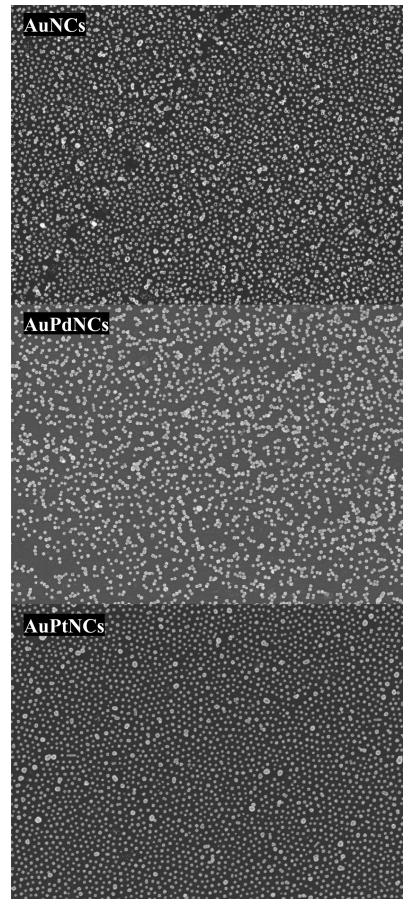


**Figure 2.** SEM images of a LB monolayer assembled on the surface of a quartz substrate at a surface pressure of the trough of 2 mN/m for the (A) gold nanocage, (B) gold–palladium double-shell nanoparticle, and (C) gold–platinum double-shell nanoparticle.

reactions, each step proceeds at a certain electrochemical potential. The reduction of 4NTP by BH is a promising system to study the different catalytic performance on the surface of gold in hollow nanoparticles when platinum or palladium is combined as an inner shell. SERS was used to monitor the reduction stages of the 4NTP bound to the surface of AuNCs, AuPdNCs, and AuPtNCs. The Raman signal is expected to come primarily from the molecules adsorbed on the gold because the surface enhancement tails off quickly with distance. Figure 3A–C show the SERS spectra of 4NTP bound to the surface of AuNC, AuPtNC, and AuPdNC monolayers on the surface of quartz substrates after being exposed to BH solution with various time delays. The SERS spectrum measured immediately after adding the BH solution corresponds to pure 4NTP, which has SERS bands at 1570 and 1331 cm<sup>-1</sup>, which are assigned to  $\nu(\text{CC})$  and  $\nu_s(\text{NO}_2)$  modes, respectively. After the reaction proceeded for a short time, new SERS bands appeared at 1431 and 1387 cm<sup>-1</sup>, corresponding to  $\nu(-\text{N}=\text{N}-)$  of the intermediate dimer. When the reaction proceeded further, the 4NTP bands decreased with time, and a band at 1594 cm<sup>-1</sup> corresponding to  $\nu(\text{CC})$  for 4ATP<sup>27</sup> increased. The band intensities are plotted against time in Figure 3D–F. The SERS band intensities were calculated after subtracting the background spectrum, which is located under the SERS spectrum. First origin software was used to create the baseline, and the intensity of the peak was measured in the middle from the baseline to the maximum point. In order to determine the

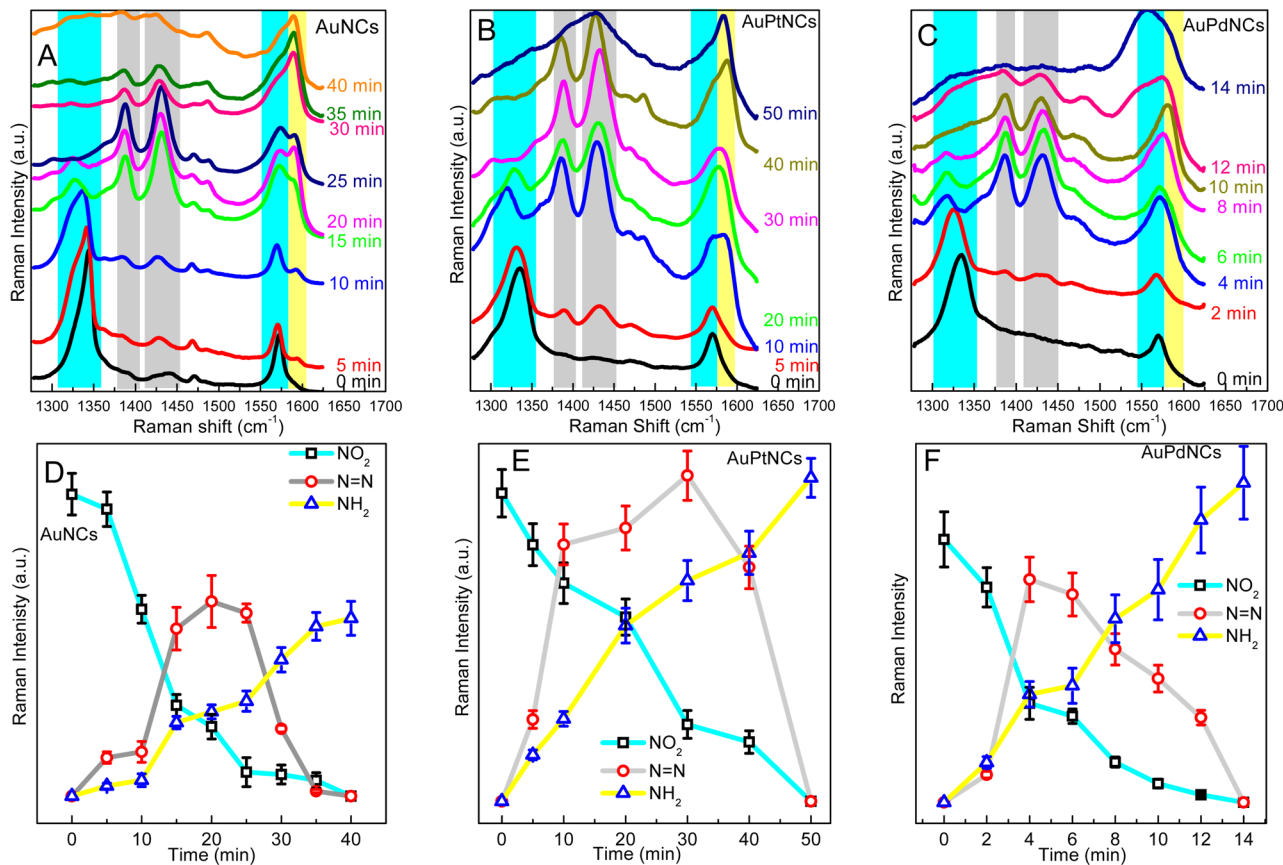


**Figure 3.** Surface-enhanced Raman spectrum collected at different times during the BH reduction of 4NTP reaction when catalyzed by a LB monolayers on the surface of a quartz substrate from (A) gold nanocages (AuNCs), (B) gold–platinum double-shell nanoparticles (AuPtNCs), and (C) gold–palladium double-shell nanoparticles (AuPdNCs). For better observation of the changes that take place on the surface of the nanoparticles, the time-dependent formation of the intermediate and product and disappearance of the reactant for the reduction of 4NTP by sodium BH were calculated from band intensities of the SERS spectrum using (D) AuNCs, (E) AuPtNCs, and (F) AuPdNCs.

intensity of the SERS band of the product, the band at  $\sim 1590 \text{ cm}^{-1}$  was deconvoluted into two bands because the reactant has a SERS band interfering with that of an amino product. For all three hollow nanocatalysts, the product and intermediate formed simultaneously. Initially, the rate of formation of the intermediate was higher than that of the product. However, when the concentration of the intermediate reached a threshold amount, it further reduced into the final product (Figure 3D–F). It is important to highlight the low value of the band intensity of the final product compared with the band intensities of the reactant and the intermediate compound in the case of using AuNCs, especially when the band intensities are compared at their maximum value. The opposite trend was observed when using AuPdNCs or AuPtNCs; the band intensities of the final product are higher than that of the reactant. One plausible reason for this result is based on the fact that there are two different mechanisms for SERS enhancement, electromagnetic and chemical. The chemical enhancement mechanism depends on the charge transfer between the adsorbed molecules and the nanoparticles, which is expected to be high in the case of AuPtNCs and AuPdNCs.<sup>11</sup> The electromagnetic mechanism depends on the strength of the plasmon field. AuNCs have strong plasmonic fields; therefore, the Raman signal enhancement is related to the electromagnetic mechanism.<sup>11</sup> Because different vibrational modes are affected differently by the two SERS mechanisms, it is reasonable to think that they are amino. In summary, the

SERS measurements showed that the 4NTP-BH, when catalyzed by the AuNC surface in the presence and absence of the platinum and palladium inner shell, proceeds through the azo dimer intermediate, which is further reduced to an amino compound via a thermal mechanism. We ensured that the photochemical reaction did not occur by using low laser frequency. Additionally, when the 4NTP adsorbed on the surface of AuNCs, AuPdNCs, and AuPtNCs was exposed to the laser in the absence of BH, no change in the SERS spectrum was observed with time (see Figure S2, Supporting Information).

**Kinetics of Catalysis with Hollow Nanoparticles.** The Raman measurements succeeded to present information about the reduction of 4NTP by BH on the surface of the single gold nanoshell and when platinum and palladium are combined with gold as an inner shell. Time-dependent band intensities corresponding to the product and reactant in the Raman spectrum shown in Figure 3 were used to study the kinetics of the reduction reaction. The catalytic study was limited to focus on the catalysis on the surface of gold nanoshells, as we planned, because the plasmon field is concentrated on the surface of gold.<sup>11</sup> The concentration of BH used during the reduction reaction was of sufficient excess to make the reduction of 4NTP pseudo-first-order. In order to confirm the order of the reaction, the first-order expression was examined for both the appearance of the product and disappearance of the reactant; straight lines were obtained.

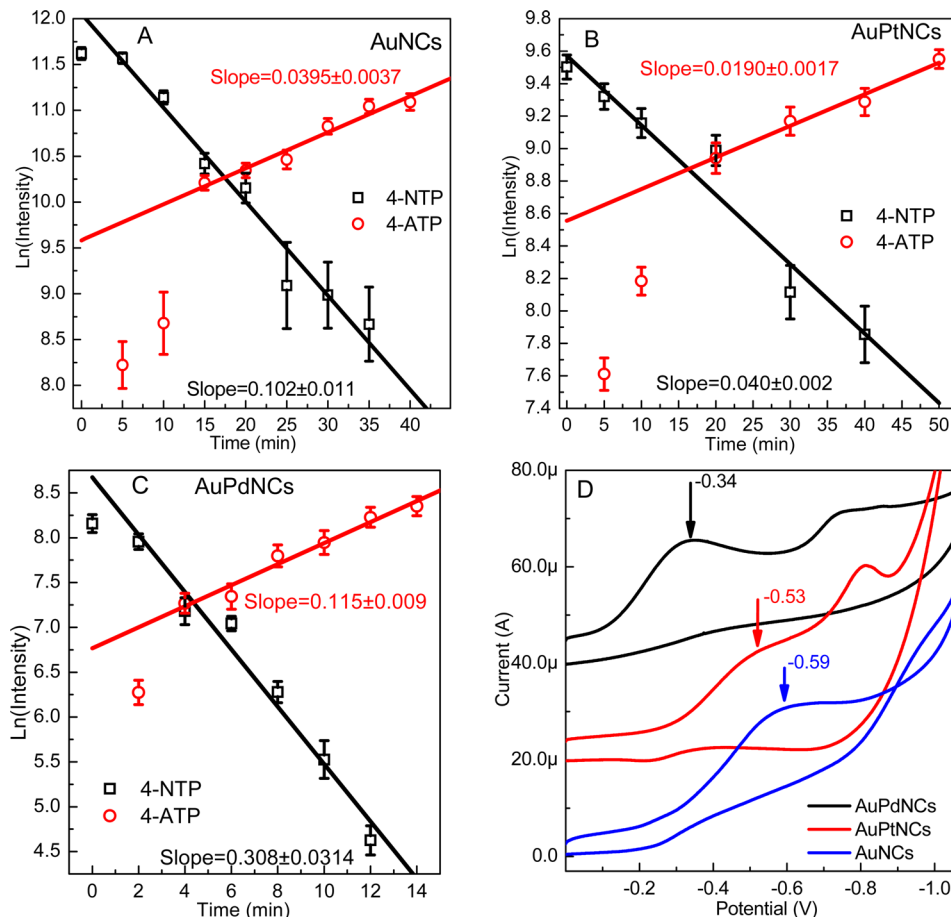


**Figure 4.** Linear relationship between the natural logarithm of the SERS band intensity of the 4NTP (reactant) and 4ATP (product) and the reaction time for the (A) AuNCs, (B) AuPtNCs, and (C) AuPdNCs. The slope of the straight line is the rate constant, which was found to be increased in the following order, AuPdNCs, AuNCs, and AuPtNCs, for both the reactant and product. (D) Cyclic voltammogram for the reduction of 4NTP on the surface of AuNCs, AuPtNCs, and AuPdNCs in 0.5 M  $\text{H}_2\text{SO}_4$ . The reduction potential increases the order of AuPdNCs, AuPtNCs, and AuNCs.

Figure 4A–C shows the linear relationship between the natural logarithm of the SERS band intensity of the 4NTP and 4ATP versus time calculated for AuNCs, AuPtNCs, and AuPdNCs, respectively. The slope of these linear expressions yields the apparent rate constant for the particular concentration of BH. The order of the reaction was confirmed by examining the second-order graph because two molecules of 4NTP were involved in the reaction to form the intermediate dimer. The second-order plot, which is the relationship between the reciprocal of the Raman band intensity of either 4NTP or 4ATP and the time of the reaction, did not fit linearly for all three nanocatalysts; see Figure S3A–C, Supporting Information.

In traditional colloidal nanocatalysis, the values of the reaction rate constant depend on the concentration of the nanoparticles, which makes it difficult to compare the catalytic efficiencies using the value of the rate constants. As known, when the concentration is increased, the probability of collision with the surface of the catalyst increases, which an increase in the value of the rate of the reaction. Interestingly, in our experiment, the reactant is chemically bound to the surface of the nanocatalysts, and the coverage density of the reactant on the gold surface is fixed; therefore, the reaction rate constants can be used in the comparison of the catalytic efficiency. The values of the rate constants of the appearance of the product

**Table 1. Rate Constant  $K$  for the Formation of Product and Disappearance of Reactant and Oxidation and Reduction Potentials (vs the AgCl/Ag electrode) Observed from CV Measurements for 4NTP Reduction by Sodium BH in the Presence of Different Nanocages**

catalyst	rate constant of reactant ( $K_{\text{Re}} \cdot \text{min}^{-1}$ )	rate constant of product ( $K_{\text{Re}} \cdot \text{min}^{-1}$ )	reduction potential (V)
AuPtNCs	$0.040 \pm 0.002$	$0.0190 \pm 0.0017$	0.53
AuNCs	$0.102 \pm 0.011$	$0.0395 \pm 0.0037$	0.59
AuPdNCs	$0.308 \pm 0.031$	$0.1150 \pm 0.0090$	0.34

and the disappearance of the reactants are reported in Table 1. In all cases herein studied, the value of the appearance rate constant was found to be half of the disappearance rate constant. This supports the idea that the reaction proceeds in two stages through formation of a persistent intermediate. The second exciting observation is that the relative values of the rate constants proceed as AuPdNCs > AuNCs > AuPtNCs. This can be attributed to the alloying of gold and palladium. As seen in Figure 1C, the interfacial layer between the Pt and Au in the AuPtNCs is rough, and there is no alloy layer as in the case of AuPdNCs.<sup>28</sup> The AuPd alloy has a density of states that is intermediate between Au and Pd. Because Pd has a greater density of states than gold, the alloy will be more active than unalloyed gold.<sup>29</sup> The reason that the Pt shell reduces the

catalytic efficiency of the Au nanoshell is attributed to the electron withdrawal effect of the Pt atoms from Au atoms.<sup>29</sup>

In order to confirm the effect of the inner Pt or Pd nanoshell on the catalytic activity of the Au outer surface in the double-shell nanocatalysts, the electrocatalytic reduction of 4NTP on the surface of AuNCs, AuPtNCs, and AuPdNCs was examined by cyclic voltammetry. Figure 4D shows the cyclic voltammogram of the reduction of 4NTP on the surface of the double-shell nanocatalysts. It is clear that the value of the reduction potential of 4NTP follows the increasing trend of AuPdNCs < AuPtNCs < AuNCs (see Table 1). The results of the electrocatalytic measurement for AuNCs and AuPdNCs agreed well with the kinetic results and supported the presence of a new Fermi level in the case of AuPdNCs, which lowered the value of the reduction potential, while the value of the reduction potential of 4NTP on the surface of AuPtNCs was found to be slightly lower than that on the surface of AuNCs. This is because unlike the regular catalysis followed by Raman spectroscopy, which senses the catalysis on the surface of the Au nanoshell, electrocatalysis measures the catalysis on the surfaces of both gold and platinum. The lattice strain that occurs between the platinum and gold nanoshells resulting from the lattice mismatch will also enhance the electrocatalytic properties of AuPtNCs.<sup>30,31</sup>

In conclusion, the mechanism of heterogeneous redox catalysis on the surface of gold nanoshells was spectroscopically studied. The surface-enhanced Raman measurement made it possible to detect any small change that took place on the surface of the catalyst and monitor the rate of reaction due to the presence of the plasmonic gold surface. The effect of introducing platinum and palladium inner shells on the catalytic efficiency of the gold outer shell was discussed. The palladium inner nanoshell was found to increase the catalytic efficiency of the gold surface, while the platinum nanoshell did the opposite. The reason for enhancing the catalytic efficiency of the gold nanoshell by introducing an inner palladium nanoshell was the formation of a palladium–gold nanoalloy layer between the pure palladium and gold nanoshells. This alloy layer has a new Fermi level of high density of states that increases the reactivity of the gold–palladium double-shell nanocatalyst. This alloy layer was not observed in the case of gold–platinum double-shell nanocatalysts, but a rough interface layer was observed instead. The unfavorable mixing between gold and platinum layers decreased the catalytic performance of the gold–platinum double-shell nanocatalyst. In order to increase the accuracy of the catalysis study, the catalysts were assembled into a monolayer on the surface of a quartz substrate, and the reactant was allowed to bind strongly with the surface of the gold nanocatalysts. Cyclic voltammetry was used to confirm the presence of the Fermi level in the case of the gold–palladium double-shell nanocatalyst.

## ■ ASSOCIATED CONTENT

### S Supporting Information

Figure S1 gives the localized surface plasmon resonance extinction spectrum of the nanocatalysts after assembly into a monolayer on the surface of quartz substrate. Figure S2 shows the surface-enhanced Raman spectrum measured for 4-nitrothiophenol adsorbed on the surface of the monolayer of the nanocatalysts after Raman laser irradiation for different times. Figure S3 is a second-order graph for the catalytic reduction of 4-nitrothiophenol by borohydride when catalyzed

by AuNCs, AuPtNCs, and AuPdNCs. This material is available free of charge via the Internet at <http://pubs.acs.org>.

## ■ AUTHOR INFORMATION

### Corresponding Author

\*E-mail: melsayed@gatech.edu.

### Notes

The authors declare no competing financial interest.

## ■ ACKNOWLEDGMENTS

This work was supported by the NSF grant (1306269).

## ■ REFERENCES

- Lewis, L. N.; Lewis, N. Platinum-Catalyzed Hydrosilylation-Colloid Formation as the Essential Step. *J. Am. Chem. Soc.* **1986**, *108*, 7228–7231.
- Freund, P. L.; Spiro, M. Colloidal Catalysis — The Effect of Sol Size and Concentration. *J. Phys. Chem.* **1985**, *89*, 1074–1077.
- Roux, R. M.; Song, H.; Hoefelmeyer, J. D.; Yang, P.; Somorjai, G. A. High-Surface-Area Catalyst Design: Synthesis, Characterization, and Reaction Studies of Platinum Nanoparticles in Mesoporous SBA-15 Silica. *J. Phys. Chem. B* **2005**, *109*, 2192–2202.
- Narayanan, R.; El-Sayed, M. A. Shape-Dependent Catalytic Activity of Platinum Nanoparticles in Colloidal Solution. *Nano Lett.* **2004**, *4*, 1343–1348.
- Abbet, S.; Ferrari, A. M.; Giordano, L.; Pacchioni, G.; Häkkinen, H.; Landman, U.; Heiz, U. Pd/MgO: A Model System in Nanocatalysis. *Surf. Sci.* **2002**, *514*, 249–255.
- Burda, C.; Chen, X. B.; Narayanan, R.; El-Sayed, M. A. Chemistry and Properties of Nanocrystals of Different Shapes. *Chem. Rev.* **2005**, *105*, 1025–1102.
- Narayanan, R.; El-Sayed, M. A. Changing Catalytic Activity During Colloidal Platinum Nanocatalysis Due to Shape Changes: Electron-Transfer Reaction. *J. Am. Chem. Soc.* **2004**, *126*, 7194–7195.
- Mahmoud, M. A.; Saira, F.; El-Sayed, M. A. Experimental Evidence for the Nanocage Effect in Catalysis with Hollow Nanoparticles. *Nano Lett.* **2010**, *10*, 3764–3769.
- Mahmoud, M. A.; El-Sayed, M. A. Time Dependence and Signs of the Shift of the Surface Plasmon Resonance Frequency in Nanocages Elucidate the Nanocatalysis Mechanism in Hollow Nanoparticles. *Nano Lett.* **2011**, *11*, 946–953.
- Mahmoud, M. A.; Narayanan, R.; El-Sayed, M. A. Enhancing Colloidal Metallic Nanocatalysis: Sharp Edges and Corners for Solid Nanoparticles and Cage Effect for Hollow Ones. *Acc. Chem. Res.* **2013**, *46*, 1795–1805.
- Mahmoud, M. A. Surface-Enhanced Raman Spectroscopy of Double-Shell Hollow Nanoparticles: Electromagnetic and Chemical Enhancements. *Langmuir* **2013**, *29*, 6253–6261.
- Sun, Y. G.; Mayers, B.; Xia, Y. N. Metal Nanostructures with Hollow Interiors. *Adv. Mater.* **2003**, *15*, 641–646.
- Yadav, M.; Akita, T.; Tsumori, N.; Xu, Q. Strong Metal–Molecular Support Interaction (SMMSI): Amine-Functionalized Gold Nanoparticles Encapsulated in Silica Nanospheres Highly Active for Catalytic Decomposition of Formic Acid. *J. Mater. Chem.* **2012**, *22*, 12582–12586.
- Park, J. C.; Bang, J. U.; Lee, J.; Ko, C. H.; Song, H. Ni@SiO<sub>2</sub> Yolk-Shell Nanoreactor Catalysts: High Temperature Stability and Recyclability. *J. Mater. Chem.* **2010**, *20*, 1239–1246.
- Chen, C.; Kang, Y. J.; Huo, Z. Y.; Zhu, Z. W.; Huang, W. Y.; Xin, H. L. L.; Snyder, J. D.; Li, D. G.; Herron, J. A.; Mavrikakis, M.; et al. Highly Crystalline Multimetallic Nanoframes with Three-Dimensional Electrocatalytic Surfaces. *Science* **2014**, *343*, 1339–1343.
- Zeng, J.; Zhang, Q.; Chen, J. Y.; Xia, Y. N. A Comparison Study of the Catalytic Properties of Au-Based Nanocages, Nanoboxes, and Nanoparticles. *Nano Lett.* **2010**, *10*, 30–35.
- Weng, G.; Mahmoud, M. A.; El-Sayed, M. A. Nanocatalysts Can Change the Number of Electrons Involved in Oxidation–Reduction

- Reaction with the Nanocages Being the Most Efficient. *J. Phys. Chem. C* **2012**, *116*, 24171–24176.
- (18) Yen, C. W.; Mahmoud, M. A.; El-Sayed, M. A. Photocatalysis in Gold Nanocage Nanoreactors. *J. Phys. Chem. A* **2009**, *113*, 4340–4345.
- (19) De la Hoz, J. M. M.; Balbuena, P. B. Geometric and Electronic Confinement Effects on Catalysis. *J. Phys. Chem. C* **2011**, *115*, 21324–21333.
- (20) Eddaoudi, M.; Kim, J.; Rosi, N.; Vodak, D.; Wachter, J.; O'Keeffe, M.; Yaghi, O. M. Systematic Design of Pore Size and Functionality in Isoreticular MOFs and Their Application in Methane Storage. *Science* **2002**, *295*, 469–472.
- (21) Graeser, M.; Pippel, E.; Greiner, A.; Wendorff, J. H. Polymer Core–Shell Fibers with Metal Nanoparticles as Nanoreactor for Catalysis. *Macromolecules* **2007**, *40*, 6032–6039.
- (22) Macdonald, J. E.; Bar Sadan, M.; Houben, L.; Popov, I.; Banin, U. Hybrid Nanoscale Inorganic Cages. *Nat. Mater.* **2010**, *9*, 810–815.
- (23) Rodríguez-Lorenzo, L.; Álvarez-Puebla, R. A.; Pastoriza-Santos, I.; Mazzucco, S.; Stéphan, O.; Kociak, M.; Liz-Marzán, L. M.; García de Abajo, F. J. Zeptomol Detection through Controlled Ultrasensitive Surface-Enhanced Raman Scattering. *J. Am. Chem. Soc.* **2009**, *131*, 4616–4618.
- (24) Heck, K. N.; Janesko, B. G.; Scuseria, G. E.; Halas, N. J.; Wong, M. S. Using Catalytic and Surface-Enhanced Raman Spectroscopy-Active Gold Nanoshells to Understand the Role of Basicity in Glycerol Oxidation. *ACS Catal.* **2013**, *3*, 2430–2435.
- (25) Li, J. F.; Huang, Y. F.; Ding, Y.; Yang, Z. L.; Li, S. B.; Zhou, X. S.; Fan, F. R.; Zhang, W.; Zhou, Z. Y.; WuDe, Y.; Ren, B.; Wang, Z. L.; Tian, Z. Q. Shell-Isolated Nanoparticle-Enhanced Raman Spectroscopy. *Nature* **2010**, *464*, 392–395.
- (26) Zhao, L.-B.; Huang, Y.-F.; Liu, X.-M.; Anema, J. R.; Wu, D.-Y.; Ren, B.; Tian, Z.-Q. A DFT Study on Photoinduced Surface Catalytic Coupling Reactions on Nanostructured Silver: Selective Formation of Azobenzene Derivatives from Para-Substituted Nitrobenzene and Aniline. *Phys. Chem. Chem. Phys.* **2012**, *14*, 12919–12929.
- (27) Yin, P. G.; Jiang, L.; You, T. T.; Zhou, W.; Li, L. D.; Guo, L.; Yang, S. H. Surface-Enhanced Raman Spectroscopy with Self-Assembled Cobalt Nanoparticle Chains: Comparison of Theory and Experiment. *Phys. Chem. Chem. Phys.* **2010**, *12*, 10781–10785.
- (28) Tran, D. T.; Johnston, R. L. Study of 40-Atom Pt–Au Clusters Using a Combined Empirical Potential-Density Functional Approach. *Proc. R. Soc. A* **2011**, *467*, 2004–2019.
- (29) Ramirez-Caballero, G. E.; Balbuena, P. B. Confinement Effects on Alloy Reactivity. *Phys. Chem. Chem. Phys.* **2010**, *12*, 12466–12471.
- (30) Hammer, B.; Norskov, J. K. Why Gold Is the Noblest of All the Metals. *Nature* **1995**, *376*, 238–240.
- (31) Strasser, P.; Koh, S.; Anniev, T.; Greeley, J.; More, K.; Yu, C.; Liu, Z.; Kaya, S.; Nordlund, D.; Ogasawara, H.; et al. Lattice-Strain Control of the Activity in Dealloyed Core–Shell Fuel Cell Catalysts. *Nat. Chem.* **2010**, *2*, 454–460.